Basal Activation of the P2X$_7$ ATP Receptor Elevates Mitochondrial Calcium and Potential, Increases Cellular ATP Levels, and Promotes Serum-independent Growth

Elena Adinolfi, Maria Giulia Callegari, Davide Ferrari, Chiara Bolognesi, Mattia Minelli, Mariusz R. Wieckowski, Paolo Pinton, Rosario Rizzuto, and Francesco Di Virgilio

Department of Experimental and Diagnostic Medicine, Section of General Pathology, and Interdisciplinary Center for the Study of Inflammation, University of Ferrara, 44100 Ferrara, Italy

P2X$_7$ is a bifunctional receptor (P2X$_7$R) for extracellular ATP that, depending on the level of activation, forms a cation-selective channel or a large conductance nonselective pore. The P2X$_7$R has a strong proapoptotic activity but can also support growth. Here, we describe the mechanism involved in growth stimulation. Transfection of P2X$_7$R increases resting mitochondrial potential ($\Delta\psi_{mt}$), basal mitochondrial Ca^{2+} ([Ca^{2+}]$_{mt}$), intracellular ATP content, and confers ability to grow in the absence of serum. These changes require a full pore-forming function, because they are abolished in cells transfected with a mutated P2X$_7$R that retains channel activity but cannot form the nonselective pore, and depend on an autocrine/paracrine tonic stimulation by secreted ATP. On the other hand, sustained stimulation of P2X$_7$R causes a $\Delta\psi_{mt}$ drop, a large increase in [Ca^{2+}]$_{mt}$, mitochondrial fragmentation, and cell death. These findings reveal a hitherto undescribed mechanism for growth stimulation by a plasma membrane pore.

INTRODUCTION

The P2X$_7$ receptor (P2X$_7$R) is a plasma membrane, ligand-gated channel that upon sustained stimulation by its physiological ligand (extracellular ATP), causes the opening of a large nonselective membrane pore (Di Virgilio, 1995; Surprenant et al., 1996; Rassendren et al., 1997). On the contrary, stimulation with low agonist concentrations triggers the transient opening of a channel with low selectivity for mono and divalent cations. The P2X$_7$R is mainly expressed in immune cells where it couples to numerous effector functions, including rapid release of interleukin-1β via microvesicle shedding, plasma membrane blebbing, macrophage fusion, lymphoid cell proliferation, and apoptotic or necrotic cell death (Di Virgilio et al., 2001; North, 2002; Burnstock, 2002). Although the role of P2X$_7$R as a cytotoxic receptor is well established, this receptor paradoxically also supports growth (Baricordi et al., 1999). Furthermore, some tumors express P2X$_7$R to a high level (Adinolfi et al., 2002;

Slater et al., 2004). The biochemical basis of the growth-stimulating activity of P2X$_7$R is unknown. We noticed that cells transfected with the P2X$_7$R showed a high level of accumulation of the potential sensitive mitochondrial dye tetramethylrhodamine methyl ester (TMRM) (Adinolfi, Rizzuto, and Di Virgilio, unpublished observation). Here, we strengthen this preliminary observation by measuring mitochondrial potential ($\Delta\psi_{mt}$), mitochondrial Ca^{2+} ([Ca^{2+}]$_{mt}$), and cellular ATP content in several clones of HEK293 cells stably transfected with the human P2X$_7$R (HEK293-hP2X$_7$R). As control we used human embryonic kidney (HEK)293 cells transfected with the empty vector (HEK293-mock) or with a defective P2X$_7$R. Our data show that transfection of the P2X$_7$R increases cellular energy stores, thus conferring a growth advantage. However, if maximally stimulated with ATP the P2X$_7$R shifts from a growth-promoting to a proapoptotic receptor, causing a massive Ca^{2+} overload of the mitochondria, disruption of the mitochondrial network, and cell death. These observations describe a mechanism whereby a plasma membrane ligand-gated pore can act either as a growth-promoting or a death-inducing receptor.

MATERIALS AND METHODS

Reagents

ATP was from Roche (Basel, Switzerland). Apyrase grade VI, oxidized ATP (oATP), and benzoyl ATP (BzATP) were purchased from Sigma-Aldrich (St. Louis, MO). TMRM (Molecular Probes, Leiden, The Netherlands) was dissolved in methanol to obtain a 10 mM stock solution and then diluted in the appropriate buffer. Carbonyl cyanide a-[3-(2-benzothiazolyl)6-[2-[2-[bis(carboxymethyl)amino]-5-methylphenoxy]-2-oxo-2H-1-benzopyran-7yl]-b-(carboxymethyl)-tetrapotassium salt (FCCP) (Sigma-Aldrich) was solubilized in ethanol to a final stock concentration of 10 mM.

Cell Culture and Transfections

HEK293 and HeLa cells were cultured in DMEM-F12 and DMEM (Sigma-Aldrich), respectively. Media were complemented with 10% heat-inactivated fetal bovine serum (FBS), 100 U/ml penicillin, and 100 mg/ml streptomycin (all from Invitrogen, San Giuliano Milanese, Italy). Stable P2X$_7$R clones were kept in the continuous presence of 0.2 mg/ml G418 sulfate (Geneticin) (Calbiochem, La Jolla, CA). Experiments, unless otherwise indicated, were performed in the following saline solution, also referred to as "standard saline" in the text: 125 mM NaCl, 5 mM KCl, 1 mM MgSO$_4$, 1 mM NaH$_2$PO$_4$, 20 mM HEPES, 5.5 mM glucose, 5 mM NaHCO$_3$, and 1 mM CaCl$_2$, pH 7.4. For Ca^{2+}-free measurements, CaCl$_2$ was omitted and 0.5 mM EGTA was added. Cells were transfected with the calcium phosphate method as described previously (Rizzuto et al., 1995; Morelli et al., 2003). All cDNAs were in pcDNA3 plasmid (Invitrogen). Green fluorescent protein and aequorin selectively targeted to the mitochondria (mtGFP and mtAEQ, respectively) were previously engineered in our laboratory. The full-length P2X$_7$R and truncated P2X$_7$R (P2X$_7$ΔCR) constructs were a kind gift of Dr. Gary Buell (Ares-Serono, Geneva, Switzerland). Stably transfected, single cell-derived clones were obtained by limiting dilution. For transient transfections cells were plated on coverslips at a 50–70% confluence, and experiments were performed 36 h later. When needed, double transfections (e.g., P2X$_7$R/mtGFP, pcDNA3.1/mtGFP) were performed at a 3:1 plasmid ratio.

Measurement of Cytosolic Ca^{2+}

Cytosolic free Ca^{2+} ([Ca^{2+}]$_i$) measurements were performed in a thermostat-controlled and magnetically stirred PerkinElmer fluorimeter with the fluorescent indicator fura-2/acetoxymethyl ester (AM) as described previously (Baricordi et al., 1999). Briefly, cells were loaded with 2 μM fura-2/AM for 30 min in the presence of 250 μM sulfinpyrazone, rinsed, and resuspended in saline solution at a final concentration of 10^6/ml. Excitation ratio and emission wavelength were 340/380 and 505 nm, respectively.

Measurement of Plasma Membrane Potential

Changes in plasma membrane potential were measured with the fluorescent dye bisoxonol (Molecular Probes) at the wavelength pair 450/580 nm, as described previously (Falzoni et al., 1995).

ATP Measurement

Total cellular ATP content was measured in aliquots of 12,500 cells seeded in microtiter plastic dishes. Cells were lysed with 10 μl of lysis buffer (FireZyme, San Diego, CA), supplemented with 100 μl of diluent buffer (FireZyme) to stabilize ATP, and placed directly into the test chamber of a luminometer (FireZyme). Then, 100 μl of a luciferin-luciferase solution was added, and light emission was recorded.

Proliferation

Cells were resuspended at the concentration of 10^5/ml in DMEM-F12 medium in the presence or absence of 10% fetal calf serum, seeded in six-well Falcon plates (BD Biosciences, Lincoln Park, NJ) and placed in a CO$_2$ incubator at 37°C. Cells were counted at various intervals in a Burker chamber with a phase-contrast Leitz microscope.

Mitochondrial Morphology

Mitochondrial morphology was analyzed in cells loaded with TMRM or transiently transfected with mtGFP. In a few experiments, cells transfected with mtGFP were loaded at the same time with TMRM to correlate mitochondrial shape and Δψ$_{mt}$. Images were acquired with a LSM 510 Zeiss confocal microscope (see below). To achieve a higher resolution of the mitochondrial network, analysis also was performed with a microscopy setup allowing image deconvolution. Images of cells transfected with mtGFP alone were acquired with a Nikon Eclipse TE300 inverted microscope (Nikon, Tokyo, Japan) equipped with a thermostated chamber (Bioptechs, Butler, PA), a 63× immersion objective, and the following filter set: excitation HQ480/40, dichroic Q480LP, and emission HQ510LP. To form a system for high-speed acquisition and processing of fluorescent images, the microscope was supplied with the following devices: a computer-controlled light shutter, a six-position filter wheel, a piezoelectric z-axis focus device, a back illuminated 1000 × 800 charge-coupled device camera (Princeton Instruments, Trenton, NJ), a computer equipped with MetaMorph software (Universal Imaging, Downingtown, PA) for image acquisition, two- and three-dimensional (3D) visualization and analysis. All experiments were performed at 37°C in the standard saline solution described in the text supplemented with 1% FBS and 2 mM glutamine. Cells transiently transfected with mtGFP and plated onto 40-mm coverslips were challenged with the appropriate stimulus and 20–25 stacks per image on z-axis were acquired at different time points. Images were then analyzed with an algorithm for 3D reconstruction developed from the Biomedical Imaging Group of the University of Massachusetts (Worcester, MA) based on point spread function analysis (Rizzuto et al., 1998).

Δψ$_{mt}$ Measurements

To measure Δψ$_{mt}$ changes, mitochondria stained with TMRM (Scaduto and Grotyohann, 1999) were imaged in single living cells by confocal microscopy. Cells, plated near confluence on 24-mm coverslips the day before, were loaded with 20 nM TMRM in standard saline solution for 30 min at 37°C. After incubation, cells were rinsed and placed in the appropriate assay buffer, always in the presence of the dye. At the concentration used, TMRM is mainly localized in the mitochondria and upon depolarization of these organelles, diffuses from mitochondria into the cytosol. To allow for nonspecific TMRM binding, measurements were routinely corrected for residual TMRM fluorescence after full Δψ$_{mt}$ collapse with the mitochondrial uncoupler FCCP (Duchen et al., 2003). Δψ$_{mt}$ was estimated by Nernst equation knowing the TMRM accumulation ratio. Confocal images were acquired with a Zeiss LSM 510 confocal microscope equipped with a plan-Apochromat 63× oil immersion objective. The 543-nm excitation wavelength was provided by a HeNe laser source. All images were obtained at a 5% laser potency and with a pinhole diameter of 1 airy unit as suggested by the manufacturer. Amplifier and detector optimizing parameters were maintained constant for all the experiments. A first set of images was obtained before stimulation with the different agonists; after addition of the stimulants, further images were acquired at 3-min intervals for 30 min. To accurately measure fluorescence emission from the entire mitochondrial network, a single 3D projection of confocal images on the z-axis was obtained by means of LSM examiner software (Carl Zeiss, Arese, Italy). Fluorescence was then quantitated and corrected for background emission with the cell imaging software Meta-Morph 2.3 (Universal Imaging). Data were acquired from 10 to 15 cells per coverslip. An average of 10 coverslips was analyzed for each experimental condition.

Measurement of Mitochondrial Ca^{2+}

[Ca^{2+}]$_{mt}$ was measured with the luminescent probe aequorin as described previously (Rizzuto et al., 1993). Briefly, 36 h after the transfection of mtAEQ (4 μg/ml), cells were incubated for 1–2 h with 5 μM coelenterazine (Molecular Probes) in the following buffer also used after for perfusion: 135 mM NaCl, 5 mM KCl, 0.4 mM KH$_2$PO$_4$, 1 mM MgSO$_4$, 20 mM HEPES, and 5.5 mM glucose, pH 7.4. Cells, plated onto 13-mm round coverslips at the density of 10^6/ml, were placed in a perfused thermostated chamber hosted in a custom-made, high-sensitivity luminometer. The light signal was collected with a low noise photomultiplier with built-in amplifier discriminator. The output of the discriminator was captured by a Thorn-EMI photon counting board and stored in an IBM-compatible computer for further analysis. The experiments were terminated by lysing the cells with 100 mM digitonin in a hypotonic Ca^{2+}-rich solution (10 mM CaCl$_2$ in H$_2$O), thus discharging the remaining AEQ pool, and the mtAEQ luminescence data were calibrated off-line into [Ca^{2+}] values by using a computer algorithm based on the Ca^{2+}-response curve of wild-type AEQ as described previously (Denton and McCormack, 1980; Rizzuto et al., 1995).

Data Analysis

All data are shown as mean ± SE of the mean. Tests of significance were performed by Student's t test by using Origin software (OriginLab, Northampton, MA).

RESULTS

HEK293 Cells Transfected with the P2X$_7$R Have a Higher Basal Δψ$_{mt}$

We performed measurements of basal Δψ$_{mt}$ in quiescent or stimulated single HEK293 cells by confocal microscopy. HEK293 cells are a very useful cell model because they do not express native receptors of the P2X family (Morelli et al., 2003). To exclude clonal selection artifacts, all the experiments were performed using several different stably transfected HEK293-hP2X$_7$R clones, of which three, named A, B, and C, are shown. All the HEK293-hP2X$_7$R clones generated in our laboratory respond to ATP stimulation with the typical P2X$_7$R "signature": 1) large and sustained Ca^{2+} influx, 2) plasma membrane potential collapse, 3) permeabilization to low-molecular-weight hydrophilic solutes, 4) swelling, and 5) membrane blebbing (our unpublished data; see also Morelli et al., 2003). As reported in Figure 1A, basal TMRM fluorescence is two- to threefold higher in the HEK293-hP2X$_7$R clones, giving a Δψ$_{mt}$ ~20–30 mV more negative than in HEK293-mock. Treatment with the P2XR blocker oATP has little effect on Δψ$_{mt}$ of HEK293-mock, but on the contrary collapses Δψ$_{mt}$ of the HEK293-hP2X$_7$R. Incubation
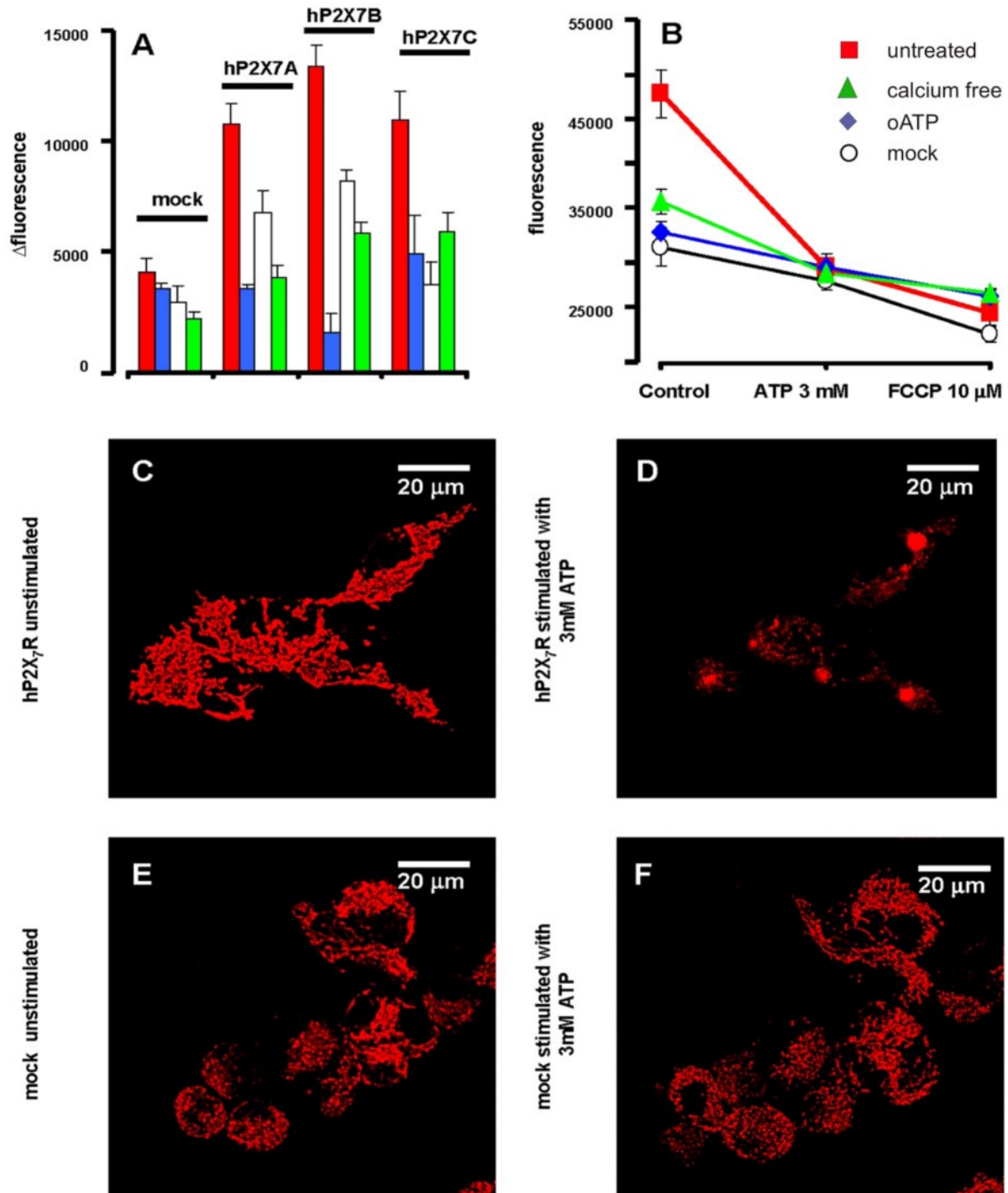
Figure 1. P2X$_7$ expression enhances resting $\Delta\psi_{mt}$ of HEK293 cells. (A) Fluorescence emission (in arbitrary units) from quiescent HEK293-mock and three stable HEK293-hP2X$_7$R clones (clone A, B, and C) loaded with the mitochondrial probe TMRM. The FCCP-insensitive fluorescence was subtracted from all values reported (Δ fluorescence) (see *Materials and Methods* for further experimental details). red, no addition; blue, 600 μM oATP for 2 h; white, 4 U/ml apyrase overnight; green, Ca^{2+} free, 0.5 mM EGTA-supplemented medium for 5 min. (B) Effect of ATP on basal $\Delta\psi_{mt}$. Fluorescence was recorded from each coverslip immediately before and 15 min after ATP addition. Finally, FCCP was added to fully collapse the $\Delta\psi_{mt}$. Parallel observations were carried out in untreated samples to check for spontaneous decay in fluorescence. Red squares, HEK293-hP2X$_7$R cells acutely incubated in standard Ca^{2+}-containing medium; green triangles, HEK293-hP2X$_7$R cells in Ca^{2+}-free, 0.5 mM EGTA-supplemented medium; blue diamonds, HEK293-hP2X$_7$R cells incubated in the presence of 600 μM oATP; white circles, HEK293-mock incubated in standard Ca^{2+}-containing medium. In B, no correction for the FCCP-insensitive fluorescence was made. Data from 10 coverslips for each condition were acquired and averaged $\pm$ SE. Difference in basal TMRM fluorescence was highly statistically significant in HEK293-hP2X$_7$R clones versus HEK293-mock ($p \leq 0.0001$, Student's *t* test). Within HEK293-hP2X$_7$R clones, difference in TMRM fluorescence in basal conditions versus oATP, or apyrase or Ca^{2+}-free conditions also was statistically significant ($p \leq 0.001$, Student's *t* test). (C–F) Confocal images of HEK293-hP2X$_7$R clone C (C and D) and HEK293-mock (E and F) loaded with 20 nM TMRM and incubated for 15 min in the absence (C and E) or presence (D and F) of 3 mM ATP.
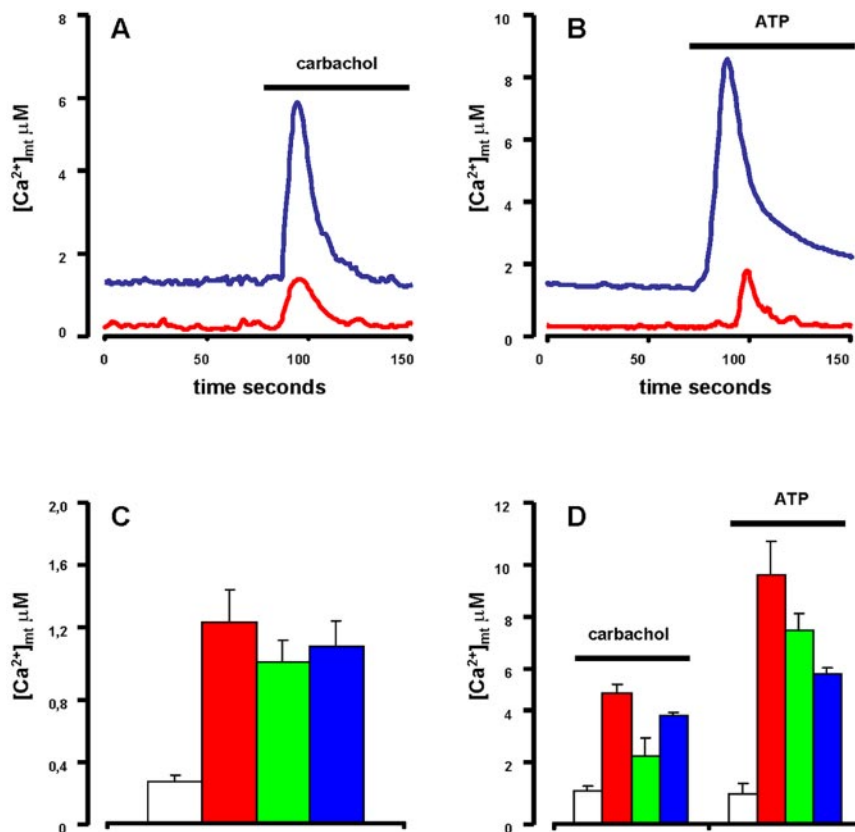
Figure 2. Transfection of the hP2X$_7$R increases both basal and stimulated [Ca^{2+}]$_{mt}$. [Ca^{2+}]$_{mt}$ levels in resting and carbachol (100 μM)- (A) or ATP (3 mM) (B)-stimulated HEK293-mock (red trace) and HEK293-hP2X$_7$R clone C (blue trace). Total counts measured at the end of each trace reading were 8,789,020 for HEK293-mock and 8,191,014 for HEK293-hP2X$_7$R (A), and 8,420,922 for HEK293-mock and 8,805,854 for HEK293-hP2X$_7$R (B). Summary data showing average ± SE resting (C) or stimulated (D) [Ca^{2+}]$_{mt}$ from 15 separate individual experiments (white, mock; red, clone A; green, clone B; blue, clone C). Basal and stimulated [Ca^{2+}]$_{mt}$ levels are significantly higher in the HEK293-hP2X$_7$R clones versus HEK293-mock (p ≤ 0.005, Student's t test). Measurements were performed with a luminometer after transient transfection of mtAEQ (see *Materials and Methods*).

with an enzyme that destroys extracellular ATP (apyrase) also decreases $\Delta\psi_{mt}$ of the HEK293-hP2X$_7$R, with little effect on that of HEK293-mock. Basal $\Delta\psi_{mt}$ is dependent on the presence of extracellular Ca^{2+} because addition of excess EGTA causes a $\Delta\psi_{mt}$ drop. These results suggest that HEK293-hP2X$_7$R cells have a higher resting $\Delta\psi_{mt}$ that seems to be dependent on the basal/tonic stimulation by endogenously released ATP and on the associated Ca^{2+} influx. These results are in keeping with previous reports showing that different cell types, among which HEK293 cells transfected with the P2X$_7$R secrete ATP (Baricordi *et al.*, 1999; Adinolfi *et al.*, 2003).

A supramaximal stimulation with 3 mM ATP (Figure 1B) causes a large $\Delta\psi_{mt}$ collapse in the HEK293-hP2X$_7$R. ATP causes a small $\Delta\psi_{mt}$ drop also in mock-transfected cells, or in HEK293-hP2X$_7$R pretreated with oATP or incubated in Ca^{2+}-free medium, suggesting that activation of other P2R also may cause a modest decrease of $\Delta\psi_{mt}$. Likely candidates are P2Y$_1$ or P2Y$_2$ that are expressed by the HEK293 cell clones used in these experiments and are coupled to Ca^{2+} release from intracellular stores (Morelli *et al.*, 2003). ATP does not fully collapse $\Delta\psi_{mt}$ because a further drop is caused by the mitochondrial uncoupler FCCP (Figure 1B). Figure 1, C–F, shows confocal fluorescence images of TMRM-loaded HEK293-hP2X$_7$R and HEK293-mock cells under quiescent or 3 mM ATP-stimulated conditions. The mitochondrial network, is bright and rather well defined in HEK293-hP2X$_7$R. ATP addition causes a large drop in fluorescence as well as mitochondrial swelling. In HEK293-mock cells, mitochondrial fluorescence is dimmer and is unaltered after ATP addition.

HEK293 Cells Transfected with the P2X$_7$R Have a Higher Basal Intramitochondrial Ca^{2+}

There is a delicate, bidirectional relationship between $\Delta\psi_{mt}$ and [Ca^{2+}]$_{mt}$ because, on the one hand, a higher $\Delta\psi_{mt}$ is expected to enhance the electrochemical gradient for Ca^{2+} transport into the mitochondria, and thus increase [Ca^{2+}]$_{mt}$ under resting or stimulated conditions, whereas on the other hand, small [Ca^{2+}]$_{mt}$ elevations cause an increase in $\Delta\psi_{mt}$. To investigate [Ca^{2+}]$_{mt}$ levels, we transfected HEK293-hP2X$_7$R and control clones with mtAEQ (Rizzuto *et al.*, 1993). Aequorin is a calcium-sensitive photoprotein that, in the presence of its cofactor coelenterazine, emits a light signal proportional to the [Ca^{2+}] of the compartment to which the probe is targeted. Figure 2A shows that resting [Ca^{2+}]$_{mt}$ is in the 100–300 nM range in mock-transfected cells. Stimulation with an extracellular stimulus coupled to Ca^{2+} mobilization from intracellular stores (charbacol) causes a transient [Ca^{2+}]$_{mt}$ rise. In HEK293-hP2X$_7$R basal [Ca^{2+}]$_{mt}$ is severalfold higher, and the increase caused by charbacol about threefold larger. Stimulation with ATP also causes a larger [Ca^{2+}]$_{mt}$ rise in the HEK293-hP2X$_7$R cells than in the HEK293-mock (Figure 2B). [Ca^{2+}]$_{mt}$ of ATP-stimulated HEK293-h P2X$_7$R returns to resting, prestimulation, levels within 5–10 min (our unpublished data). Average basal [Ca^{2+}]$_{mt}$ levels for mock-transfected and three different HEK293-hP2X$_7$R clones are reported in Figure 2C. Average [Ca^{2+}]$_{mt}$ increases stimulated by carbachol or ATP are shown in Figure 2D.

We next investigated the effect of removal of extracellular Ca^{2+} on basal and stimulated [Ca^{2+}]$_{mt}$. Basal [Ca^{2+}]$_{mt}$ level of HEK293-hP2X$_7$R was fourfold reduced, to the level of that
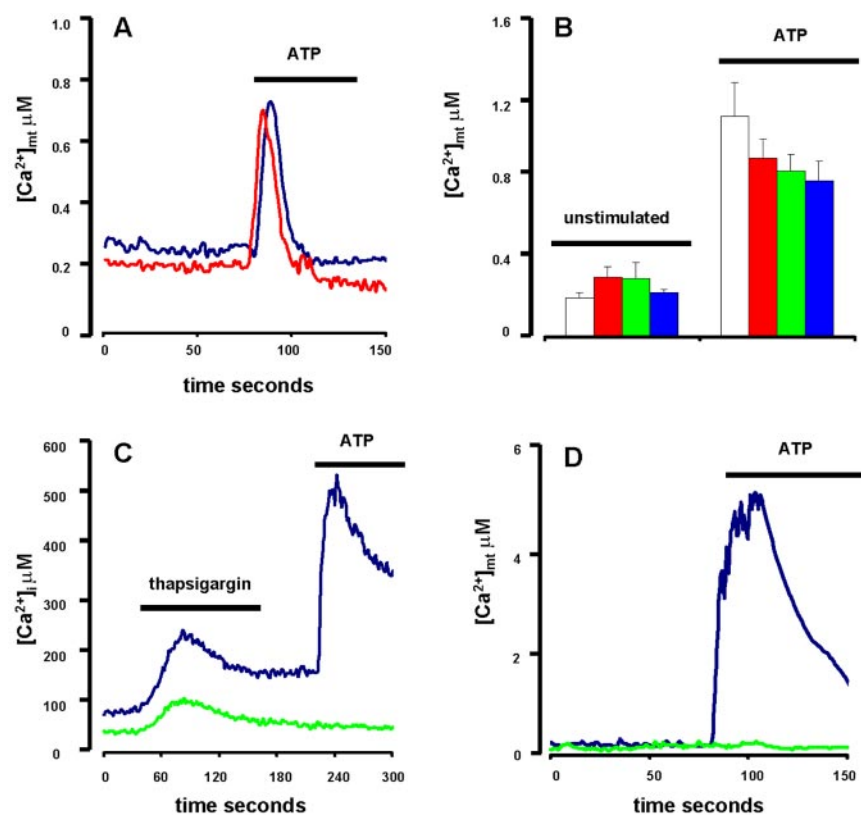
Figure 3. Effect of extracellular Ca^{2+} removal and ER Ca^{2+} stores depletion on basal and stimulated $[Ca^{2+}]_{mt}$ and $[Ca^{2+}]_i$. (A) HEK293-hP2X$_7$R clone C (blue trace) and HEK293-mock (red trace) were incubated in Ca^{2+}-free, 0.5 mM EGTA supplemented medium and stimulated with 3 mM ATP. Total counts were 8,978,844 for HEK293-hP2X$_7$R and 8,494,385 for HEK293-mock. (B) Summary data showing averages ± SE for unstimulated and ATP-stimulated cells from five separate individual experiments (white, mock; red, clone A; green, clone B; blue, clone C). Differences in basal or ATP-stimulated $[Ca^{2+}]_{mt}$ of HEK293-hP2X$_7$R clones versus HEK293-mock were not statistically significant ($p \geq 0.1$, Student's *t* test). Differences in $[Ca^{2+}]_{mt}$ between unstimulated and ATP-stimulated cells (whether HEK293-hP2X$_7$R or HEK293-mock) were statistically significant ($p \leq 0.0005$, Student's *t* test). (C and D) HEK293-hP2X$_7$R clone C incubated in Ca^{2+}-containing (blue trace) or Ca^{2+}-free, 0.5 mM EGTA-supplemented (green trace) medium. In C, cells also were loaded with 2 μM fura 2/AM. In D, cells were treated with thapsigargin for 30 min before ATP addition. Thapsigargin and ATP were 30 nM and 3 mM, respectively. In D, total counts were 8,441,325 and 8,334,432 for HEK293-hP2X$_7$R in Ca^{2+}-containing or Ca^{2+}-depleted medium, respectively. Measurements were performed with a luminometer after transient transfection of mtAEQ (A, B, and D) or with a fluorimeter (C) (see *Materials and Methods*).

of HEK293-mock, by chelation of extracellular Ca^{2+} (Figure 3, A and B). ATP-stimulated increases were unaffected in HEK293-mock and severely curtailed in HEK293-hP2X$_7$R. Similar results also were obtained with carbachol as a stimulant (our unpublished data). This suggests that in the presence of extracellular Ca^{2+} both resting and stimulated $[Ca^{2+}]_{mt}$ rise in HEK293-hP2X$_7$R cells are mainly, albeit not exclusively, dependent on influx from the extracellular space, whereas in Ca^{2+}-free medium, the $[Ca^{2+}]_{mt}$ increase depends on the uptake of Ca^{2+} mobilized from intracellular stores. Under these latter conditions, the ATP-stimulated $[Ca^{2+}]_{mt}$ phenotype of HEK293-hP2X$_7$R resembles that of HEK293-mock because in both cell types Ca^{2+} mobilization is exclusively due to stimulation of P2YR (Morelli *et al.*, 2003). Blockade of the P2X$_7$R by a 2-h incubation in the presence of 600 μM oATP reduced by 50% basal $[Ca^{2+}]_{mt}$ levels, and fully obliterated the ATP-stimulated $[Ca^{2+}]_{mt}$ rise of HEK293-hP2X$_7$R cells (our unpublished data). In these cells, participation to the ATP-dependent $[Ca^{2+}]_{mt}$ rise of Ca^{2+} transfer from the endoplasmic reticulum (ER) is further supported by the effect of thapsigargin (Figure 3, C and D). Pretreatment of HEK293-hP2X$_7$R cells with this inhibitor of ER Ca-ATPase has little effect if any on both the $[Ca^{2+}]_i$ and $[Ca^{2+}]_{mt}$ rises triggered by ATP in the presence of extracellular Ca^{2+}. In Ca^{2+}-free medium, thapsigargin treatment obliterates both the $[Ca^{2+}]_i$ and the $[Ca^{2+}]_{mt}$ rises stimulated by ATP. Figure 3D also shows that basal $[Ca^{2+}]_{mt}$ level of HEK293-hP2X$_7$R is lowered to that of HEK293-mock after a prolonged incubation in the presence of thapsigargin. Overall, the thapsigargin experiments suggest that in the HEK293-hP2X$_7$R cells the ATP-stimulated increase in $[Ca^{2+}]_{mt}$ is minimally affected by the filling status of the ER under near physiological conditions (i.e., in the presence of

extracellular Ca^{2+}). On the contrary, in the absence of extracellular Ca^{2+} the ATP-stimulated $[Ca^{2+}]_{mt}$ increase is largely dependent on the intactness of the ER Ca^{2+} stores. Finally, the elevated basal $[Ca^{2+}]_{mt}$ observed in HEK293-hP2X$_7$R in the presence of extracellular Ca^{2+} (Figure 2) depends on availability of ER Ca^{2+} because it is reduced to HEK293-mock levels by thapsigargin pretreatment.

On the basis of previous observations (Baricordi *et al.*, 1999) in LG14 lymphoblastoma and K562 erythroleukemic cell transfected with hP2X$_7$R, we anticipated a $[Ca^{2+}]_i$ level higher in HEK293-hP2X$_7$R than in HEK293-mock. However, the three HEK293-hP2X$_7$R clones used here have an average $[Ca^{2+}]_i$ level (120 ± 15, n = 15) not dissimilar from that of HEK293-mock (112 ± 13 nM, respectively, n = 6), suggesting that the enhanced basal Ca^{2+} influx through the P2X$_7$R does not cause a measurable increase in the average $[Ca^{2+}]_i$, but it is directly taken up by the ER and then transferred to the mitochondria, albeit a direct influx into the mitochondria at sites of close contact between mitochondria and the plasma membrane cannot be excluded (Rizzuto *et al.*, 2000).

Deletion of the P2X$_7$R COOH Tail Prevents Intramitochondrial Ion Changes

Sustained activation of the P2X$_7$R causes the opening of a large plasma membrane pore that admits molecules up to 900 Da. Although it is as yet unclear whether pore formation is due to the increase in size of the channel intrinsic to the receptor or to the recruitment of an additional pore-forming molecular structure distinct from the receptor itself, it is well established that pore opening depends on the intactness of the extended COOH-terminal cytoplasmic tail typical of the P2X$_7$R. Truncation at AA 416 or 418 abolishes the ability to translocate hydrophylic molecules of molecular mass higher

Figure 4. Lack of effect of rP2X$_7$ΔCR on Δψ$_{mt}$ and [Ca^{2+}]$_{mt}$. (A) TMRM fluorescence emission from HEK293-rP2X$_7$R (dark blue) or HEK293-rP2X$_7$ΔCR (cyan) incubated in Ca^{2+}-supplemented (closed symbols) or Ca^{2+}-free, 0.5 mM EGTA-containing (open symbols) medium. Fluorescence was recorded from each coverslip immediately before and 15 min after ATP addition. Finally, FCCP was added to fully collapse the Δψ$_{mt}$. Parallel observations were carried out in untreated samples to check for spontaneous decay in fluorescence. Fifteen coverslips for each condition were analyzed and averages ± SE calculated. Basal TMRM fluorescence is significantly lower in HEK293-rP2X$_7$ΔCR versus HEK293-rP2X$_7$R (p ≤ 0.001). (B) [Ca^{2+}]$_{mt}$ levels in resting and ATP-stimulated HEK293-rP2X$_7$ΔCR (cyan trace) and HEK293-rP2X$_7$R clone C (dark blue trace). Total counts measured at the end of each trace reading were 7,862,488 for HEK293-rP2X$_7$R and 7,631,450 for HEK293-rP2X $_7$ΔCR. ATP concentration was 3 mM. Summary data showing average ± SE resting (C) or ATP-stimulated (D) [Ca^{2+}]$_{mt}$, respectively, from 15 individual experiments (dark blue, HEK293-rP2X$_7$R; cyan, HEK293-rP2X$_7$ΔCR). Basal [Ca^{2+}]$_{mt}$ of HEK293-rP2X$_7$R and HEK293-rP2X$_7$ΔCR were significantly different with a p ≤ 0.001. ATP-stimulated [Ca^{2+}]$_{mt}$ of HEK293-rP2X$_7$R and HEK293-rP2X$_7$ΔCR were significantly different with a p ≤ 0.0001. (E) HEK293-rP2X$_7$R (dark blue trace), HEK293-rP2X$_7$ΔCR (cyan trace), and HEK293-mock (green trace) were loaded with 2 μM fura 2/AM and stimulated with 3 mM ATP in Ca^{2+}-containing medium. (F) HEK293-rP2X$_7$R (dark blue trace), HEK293-rP2X$_7$ΔCR (cyan trace), and HEK293-mock (green trace) were incubated in Ca^{2+}-containing medium in the presence of the membrane potential indicator 100 nM bis-oxonol and stimulated with 3 mM ATP. First and second KCl additions were 15 and 30 mM, respectively.
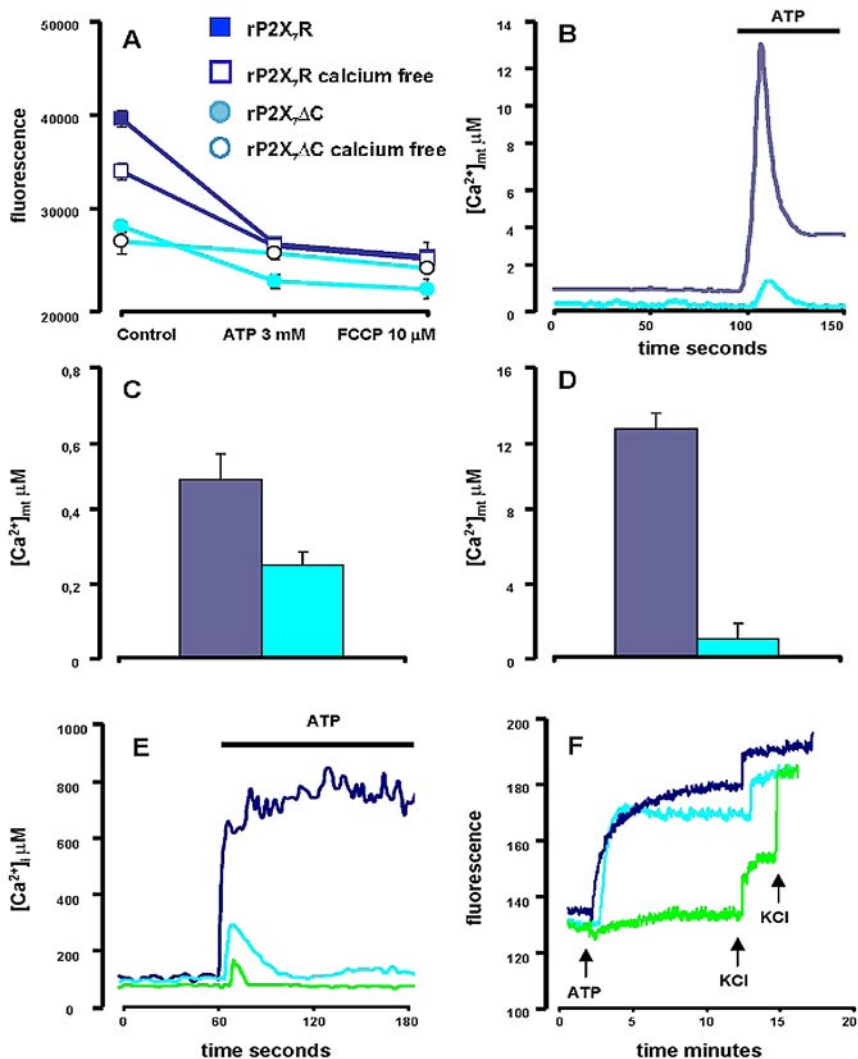
than 200 and up to 900 Da (pore function), but it does not affect conductance to small cations (Na$^+$, K$^+$, and Ca^{2+}) (Surprenant *et al.*, 1996; Rassendren *et al.*, 1997). Furthermore, the COOH tail is thought to allow interaction of P2X$_7$R with different intracellular proteins that might be involved in signal transduction (Kim *et al.*, 2001). Because hP2X$_7$ΔCR does not translocate to the plasma membrane (Ferrari *et al.*, 2004), we were forced to use the rat receptor truncated at position 415 (rP2X$_7$ΔCR). Control experiments were accordingly performed with the full length rP2X$_7$R. Figure 4A shows that also HEK293 cells transfected with the rP2X$_7$R (HEK293-rP2X$_7$R), whereas HEK293 cells transfected with the rP2X$_7$ΔCR (HEK293-rP2X$_7$ΔCR) have a much lower Δψ$_{mt}$, nonsignificantly dissimilar from that of HEK293-mock (Figure 1B). In both HEK293-rP2X$_7$R and HEK293-rP2X$_7$ΔCR chelation of extracellular Ca^{2+} causes a Δψ$_{mt}$ drop (Figure 4A). The addition of ATP causes a collapse of Δψ$_{mt}$ in cells transfected with the full length as well as the truncated receptor, larger in the former. A further small drop is induced by FCCP. Basal [Ca^{2+}]$_{mt}$ levels in the HEK293-rP2X$_7$ΔCR are about half of those in the HEK293-rP2X$_7$R (Figure 4, A and C). P2X$_7$R truncation also prevents the large ATP-stimulated [Ca^{2+}]$_{mt}$ increase observed in cells transfected with the full-length

receptor (Figure 4B). Averages [Ca^{2+}]$_{mt}$ increases are shown in Figure 4D. Lower Δψ$_{mt}$ and [Ca^{2+}]$_{mt}$ in HEK293-rP2X$_7$ΔCR might depend on lack of plasma membrane expression of this defective receptor. As no monoclonal antibodies raised against the extracellular domain of the rP2X$_7$R are currently available, to check that the rP2X$_7$ΔCR was correctly expressed on the plasma membrane, we recorded well established changes in intracellular ion homeostasis triggered by its activation by ATP (Surprenant *et al.*, 1996; Ferrari *et al.*, 2004). Figure 4E shows that ATP stimulation of HEK293-rP2X$_7$ΔCR causes a [Ca^{2+}]$_i$ increase larger than that observed in mock-transfected cells, albeit shorter and smaller compared with that observed in HEK293-rP2X$_7$R. The smaller Ca^{2+} influx is due to the much lower conductance of the small channel generated by the truncated compared with the full-length rP2X$_7$R (Surprenant *et al.*, 1996). Furthermore, HEK293-rP2X$_7$ΔCR were almost completely depolarized by ATP (Figure 4F), showing that ion conductance through the truncated receptors, albeit small, was sufficient to collapse plasma membrane potential. Plasma membrane potential changes caused by HEK293-mock and HEK293-rP2X$_7$R are shown for comparison.

Unstimulated
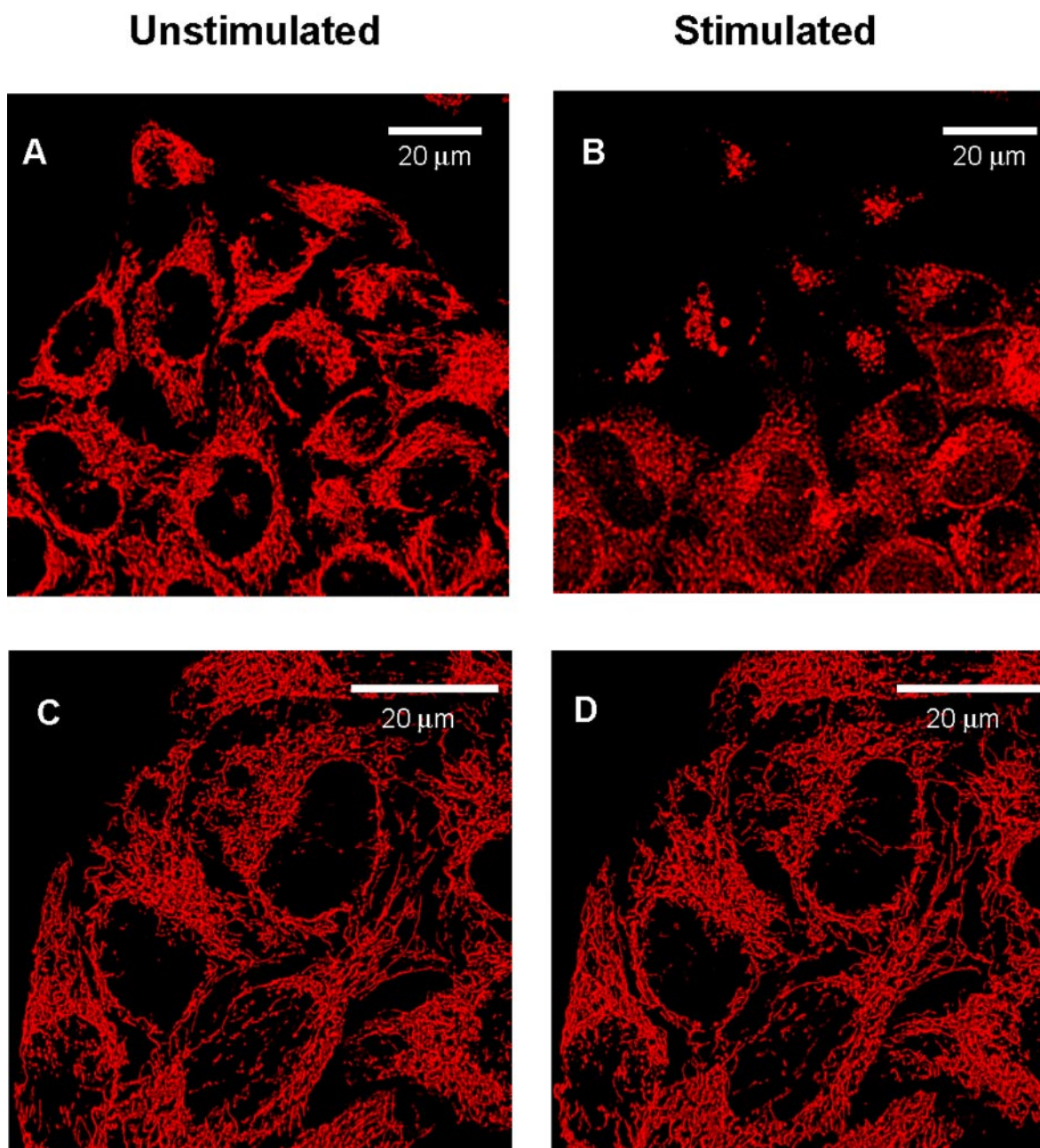
Stimulated

Figure 5. Responses of HeLa-P2X$_7$R cells to ATP stimulation. HeLa cells were transiently transfected with P2X$_7$R (A and B) or with the empty plasmid (C and D) and loaded with 20 nM TMRM. Stimulation was performed with 3 mM ATP (B and D). Images were acquired shortly before and 15 min after ATP addition. Analysis of several slides (n = 15) showed that ~58 ± 6% of HeLa cells incorporated the P2X$_7$R-containing plasmid and of these ~98 ± 15% lost TMRM fluorescence upon ATP stimulation.

Activation of the P2X$_7$R Causes Fragmentation of the Mitochondria

Changes in mitochondrial ion homeostasis are often paralleled by changes in morphology that precede changes in whole cell shape and function. In addition to HEK293-hP2X$_7$R, we also used HeLa cells transiently transfected with hP2X$_7$R (HeLa-hP2X$_7$R) because these latter cells, due to their extremely flattened morphology, allow a much better resolution of the mitochondrial network (Rizzuto *et al.*, 1995). Mitochondrial morphology was investigated in cells loaded with TMRM or transfected with the fluorescent protein mtGFP. In some experiments, mitochondria were colabeled with TMRM and mtGFP. Figure 5 shows that TMRM allows a clear definition of the mitochondrial network in HeLa cells, whether hP2X$_7$R- or mock-transfected (Figure 5, A and C). However, even under basal conditions, hP2X$_7$R expression causes a slight rounding and swelling of the mitochondria (Figure 5A). As shown previously for HEK293-hP2X$_7$R (Figure 1D), addition of ATP collapses $\Delta\psi_{mt}$ and within 10–15 min heavily fragments the mitochondrial network in HeLa-hP2X$_7$R cells (Figure 5B), but causes little if any change in control HeLa-mock (Figure 5D). Similar results also were obtained in HeLa-hP2X$_7$R transfected with mtGFP, loaded at the same time with TMRM and

Unstimulated
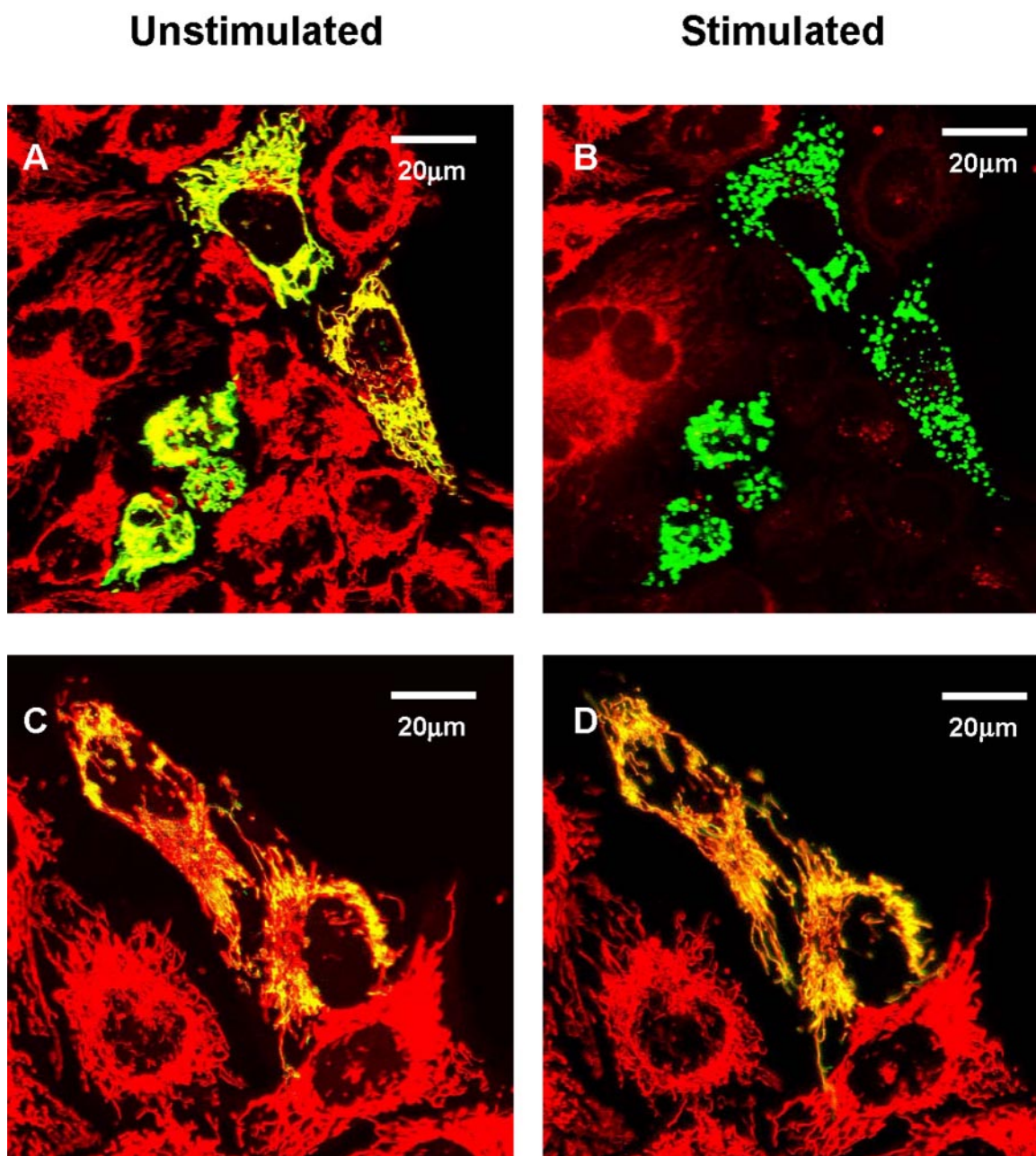
Stimulated

Figure 6. Mitochondrial morphology in P2X$_7$R and mock-transfected cells. HeLa cells were transiently transfected with P2X$_7$R/mtGFP (A and B) at a 3:1 ratio, or mtGFP alone (C and D) (see *Materials and Methods*) and loaded with TMRM. Stimulation was performed with 300 μM BzATP (B and D). Images were acquired shortly before and 15 min after BzATP addition. Percentage of P2X$_7$R- transfected cells was as in Figure 5. Percentage of mtGFP-transfected cells was 18 $\pm$ 3.

stimulated with the potent P2X$_7$ agonist BzATP (Figure 6). In these cells, morphological changes of mitochondria triggered by P2X$_7$R activation are even more striking because mtGFP is retained within the depolarized and fragmented mitochondria (Figure 6B). HeLa-mock are fully refractory to stimulation by BzATP (Figure 6D). Mitochondrial fragmentation is accompanied both in HEK293-hP2X$_7$R (Figure 7) and HeLa-hP2X$_7$R (Figure 8) by the typical membrane blebbing previously described in HEK293 and THP-1 macrophages (MacKenzie *et al.*, 2001; Morelli *et al.*, 2003) and is followed by cell death (our unpublished data). These changes do not occur in mock-transfected cells. In the ab-

sence of extracellular Ca^{2+}, the P2X$_7$R-dependent mitochondrial fragmentation is almost completely prevented, although $\Delta\psi_{mt}$ drop and some mitochondrial swelling still occurs both in HEK293-hP2X$_7$R and HeLa-hP2X$_7$R (our unpublished data).

HEK293 Cells Transfected with the P2X$_7$R Grow in the Absence of Serum and Have a Higher ATP Content
We previously showed that transfection of B lymphoblastoid and K562 cells with P2X$_7$R allows growth in the absence of serum, a feature of transformed cells (Baricordi *et al.*, 1999). All HEK293-hP2X$_7$R clones, three shown in Figure 9,

Unstimulated
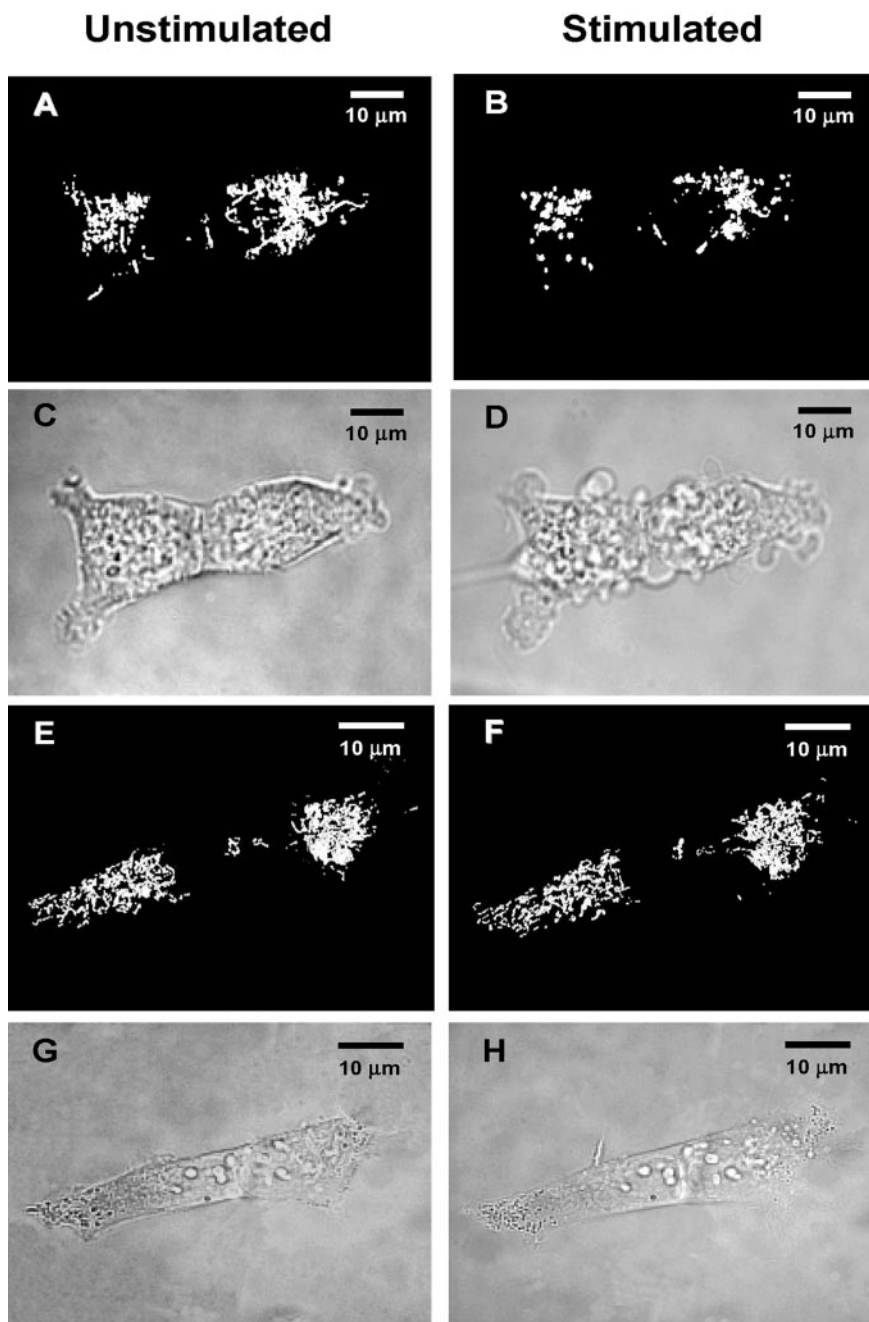
Stimulated

Figure 7. Plasma membrane blebbing occurs in parallel with mitochondrial fragmentation in HEK293-hP2X$_7$R. HEK293-hP2X$_7$R (A–D) or HEK293-mock (E–H) cells were transiently transfected with mtGFP and stimulated with 3 mM ATP. Pictures were acquired with the Nikon microscopy set up before (A, C, E, and G) and 15 min after ATP addition (B, D, F, and H), and deconvoluted (see *Materials and Methods*). Fluorescence, A, B, E, and F. Light transmission, C, D, G, and H. Percentage of mtGFP-transfected cells was 15 ± 3.

are able to proliferate in serum-free medium, in contrast to mock-transfected cells (Figure 9A). Growth is dramatically abrogated by treatment with either oATP (600 μM) (Figure 9B) or apyrase (4 U/ml) (Figure 9C). Interestingly, whereas oATP, a P2X-selective blocker, has no effect on survival of mock-transfected cells, apyrase strongly reduces their number, suggesting that P2Y$_1$ or P2Y$_2$ receptor activation may support survival of HEK293 cells. Growth advantage conferred by P2X$_7$R requires extracellular Ca^{2+} and the full-length receptor because, on the one hand, it is fully abrogated in Ca^{2+}-free medium (Figure 9D), and on the other hand, HEK293-P2X$_7$ΔCR do not proliferate in the absence of serum (Figure 9E).

There is growing consensus that [Ca^{2+}]$_{mt}$ is one of the key factors controlling ATP synthesis (Jouaville *et al.*, 1999), fur-

thermore a higher $\Delta\psi_{mt}$, by increasing the driving force for protons, also increases the efficiency of oxidative phosphorylation. Figure 10 shows that both HEK293-hP2X$_7$R and HEK293-rP2X$_7$ cells have a several fold higher ATP content (normalized to cellular protein) compared with HEK293-mock cells. On the contrary, HEK293-rP2X$_7$ΔCR cells have an ATP content not dissimilar from that of controls. Blockade of P2X$_7$R by oATP reduces cellular ATP levels to those of mock-transfected cells.

DISCUSSION

The P2X$_7$R is attracting attention as a mediator of the early phases of inflammation and as a cytotoxic, proapoptotic

Unstimulated   Stimulated
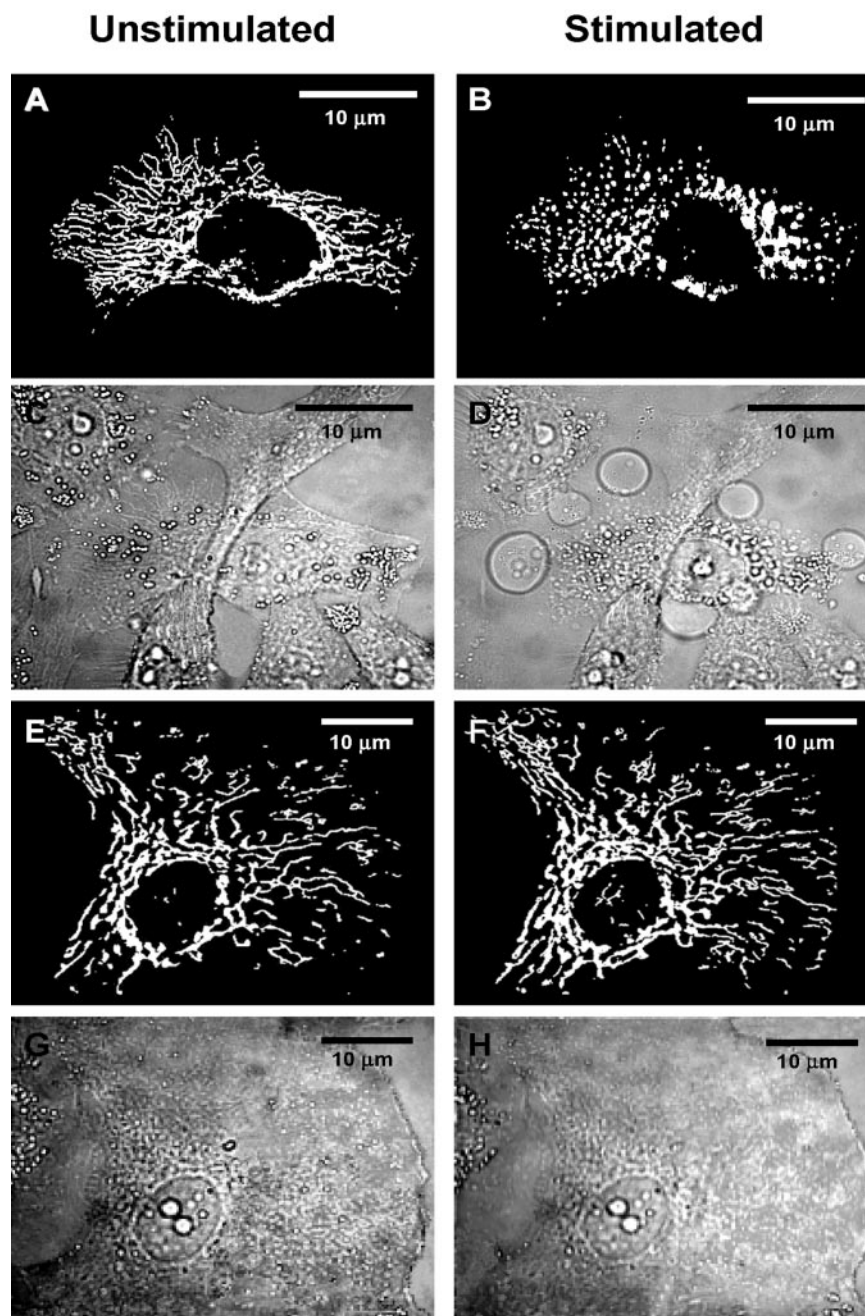
Figure 8. Plasma membrane blebbing occurs in parallel with mitochondrial fragmentation in HeLa-hP2X$_7$R. HeLa cells were transiently transfected with P2X$_7$R/mtGFP (A–D) or pcDNA3.1/mtGFP (mock) (E–H) at a 3:1 ratio and stimulated with 3 mM ATP. Images were acquired with Nikon microscopy setup before (A, C, E, and G) and 10 min after ATP addition (B, D, F, and H), and deconvoluted (see *Materials and Methods*). Fluorescence A, B, E, and F. Light transmission: C, D, G, and H. Percentage of P2X$_7$R-transfected cells was as in Figure 5. Percentage of mtGFP-transfected cells was as in Figure 6.

receptor. This reputation is not undeserved because few if any plasma membrane receptors are as potent as P2X$_7$R in the activation of IL-1β-release or of cell death (Di Virgilio *et al.*, 2001). Less appreciated is that P2X$_7$R also may stimulate growth. We originally reported that transfection of human lymphoblastoid or erythroleukemic cells with P2X$_7$R conferred ability to grow in the absence of serum (Baricordi *et al.*, 1999). Recent studies have disclosed a high expression level of this receptor in several cancers (Adinolfi *et al.*, 2002; Greig *et al.*, 2003; Slater *et al.*, 2004). This raises the question of the mechanism by which P2X$_7$R can either promote growth or trigger cell death. It is now clear that mitochondria are a crucial intersection of cell pathways leading to cell proliferation or death and thus an obvious candidate target. In cells transfected with the P2X$_7$R, we have unveiled a

number of distinct mitochondrial metabolic features that concordantly support a higher growth or survival ability.

The P2X$_7$R transfectants have higher $\Delta\psi_{mt}$, resting and stimulated $[Ca^{2+}]_{mt}$, and ATP content. Although it is likely that additional metabolic pathways also are activated in these cells, the increased level of energy stores will help these cells survive under conditions of limited supply of growth factors (e.g., serum starvation). The growth stimulus is dependent on an autocrine/paracrine purinergic loop triggered by release of endogenous ATP, because apyrase abrogates cell proliferation. It might seem surprising that the low-affinity P2X$_7$R is activated under resting conditions, because HEK293 cells were reported to release ATP in the nanomicromolar range (Adinolfi *et al.*, 2003). However, this is the average ATP concentration measured in the superna-
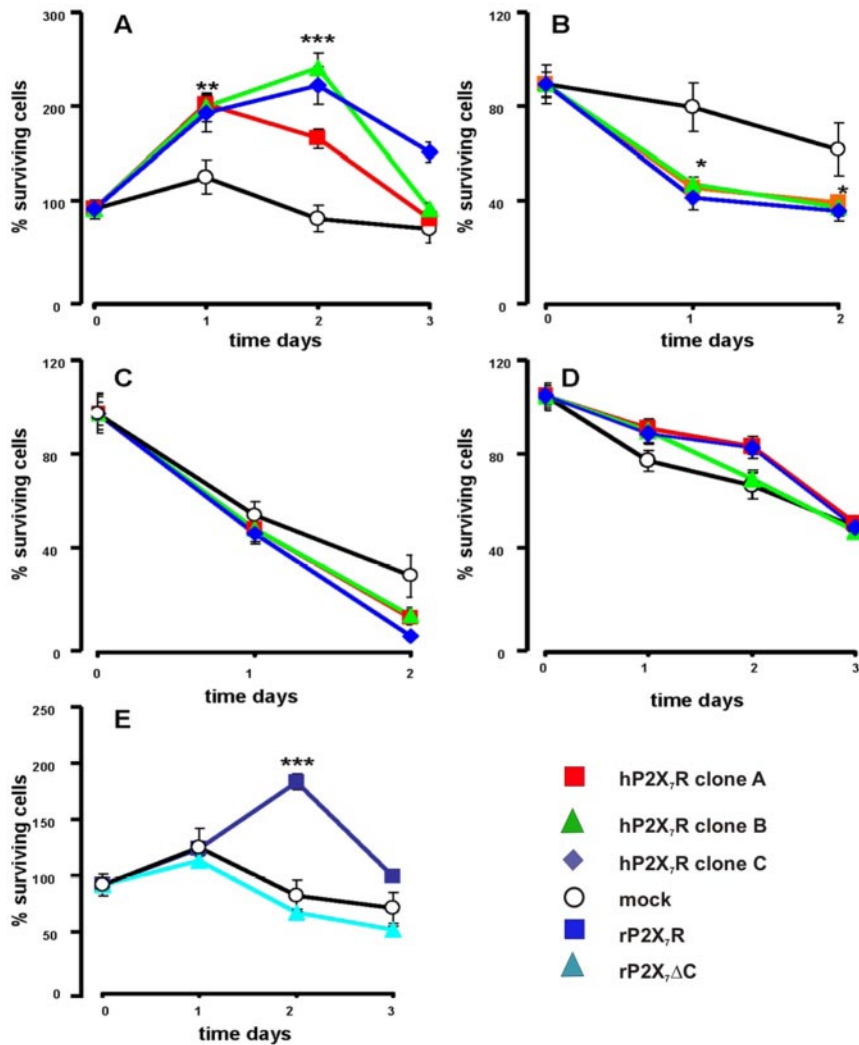
Figure 9. Transfection of the P2X$_7$R allows proliferation in the absence of serum. HEK293-mock and HEK293-hP2X$_7$R (A–C), or HEK293-rP2X$_7$R and HEK293-rP2X$_7$ΔCR cells (E) were incubated in serum-free DMEM-F12 medium for the indicated times. The medium also contained 600 μM oATP (B) or 4 U/ml apyrase (C). (D) HEK293-mock and HEK293-hP2X$_7$R were incubated in serum-free, 2 mM EGTA-supplemented DMEM medium. Coding: white circles, mock; red squares, HEK293-hP2X$_7$R clone A; green triangles, HEK293-hP2X$_7$R clone B; blue diamonds, HEK293-hP2X$_7$R clone C; dark blue squares, HEK293-rP2X$_7$ cells; cyan triangles, HEK293-rP2X$_7$ΔC. *p $\leq$ 0.01 versus HEK293-mock; **p $\leq$ 0.001 versus HEK293-mock; ***p $\leq$ 0.0001 versus HEK293-mock.

tants, i.e., once secreted ATP has diffused into and equilibrated with the extracellular medium; therefore, it only roughly reflects the actual ATP concentration reached in the vicinity of the plasma membrane. Furthermore, ATP is likely to be released at distinct plasma membrane sites where it can transiently accumulate in concentrations sufficient to activate P2X$_7$R and thus drive a paracrine/autocrine stimulatory loop (Joseph *et al.*, 2003; Fabbro *et al.*, 2004).

Ca^{2+} influx through the P2X$_7$R seems to be necessary for mitochondrial hyperpolarization as chelation of extracellular Ca^{2+} lowers $\Delta\psi_{mt}$ to the level of HEK293-mock. The link between extracellular Ca^{2+} and the $\Delta\psi_{mt}$ is likely to be the [Ca^{2+}]$_{mt}$, a parameter that is increased in HEK293-P2X$_7$R. Thus, we hypothesize that tonic P2X$_7$R activity induces a constant "leak" of Ca^{2+} across the plasma membrane into the mitochondria where it enhances the basal metabolic activity, increases $\Delta\psi_{mt}$ and stimulates ATP synthesis. It was originally shown by Denton and McCormack (1980) that pyruvate dehydrogenase, NAD$^+$-isocitrate dehydrogenase, and 2-oxoglutarate dehydrogenase are modulated by Ca^{2+}. These three enzyme complexes catalyze the formation of NADH and thus control oxidative metabolism. Rizzuto *et al.* (1994) provided direct experimental evidence that NADH production increases in parallel with the increase in [Ca^{2+}]$_{mt}$. A severalfold increase in the activity of these en-

zymes was observed for [Ca^{2+}]$_{mt}$ increases in the low micromolar range, similar to those reported in the present study. Here, we suggest that not only a transient [Ca^{2+}]$_{mt}$ increase in the micromolar range but also a sustained submicromolar [Ca^{2+}]$_{mt}$ elevation may cause an enhanced metabolic mitochondrial activity that results in activation of mitochondrial oxidative phosphorylation and higher intracellular ATP levels. The activated basal metabolic status also explains the growth advantage of the P2X$_7$R transfectants. Interestingly, in the HEK293-P2X$_7$R the increases in [Ca^{2+}]$_{mt}$ stimulated by agonists acting at G protein-coupled receptors (e.g., carbachol) is also augmented. This may confer an additional advantage to P2X$_7$R-expressing cells because they might be primed to react more efficiently to Ca^{2+}-dependent growth stimuli.

Elevated basal [Ca^{2+}]$_{mt}$ in P2X$_7$R-transfected cells might be due to several alterations in intracellular Ca^{2+} handling, such as increased influx through the plasma membrane, increased Ca^{2+} transfer from the ER to the mitochondria, or even an abnormal localization of the mitochondria. We anticipated that basal [Ca^{2+}]$_i$ also would be higher in the P2X$_7$R transfectants, but this is not the case in either HEK293-hP2X$_7$R or HEK293-rP2X$_7$R. This suggests that a higher plasma membrane Ca^{2+} influx through a tonically activated P2X$_7$R can directly be sensed by the mitochondria
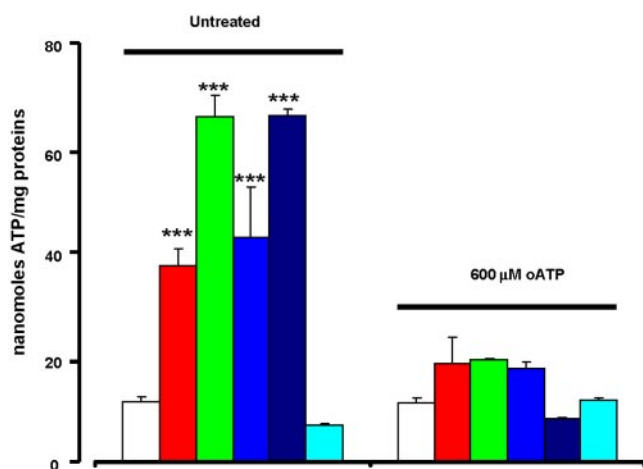
Figure 10. ATP content of HEK293-P2X$_7$R and mock-transfected cells: effect of oATP. Intracellular ATP content of mock-, hP2X$_7$R-, rP2X$_7$R-, and rP2X$_7$ΔCR-transfected cells incubated in the absence or presence of 600 μM oATP for 16 h was measured as described in *Materials and Methods*. Coding: white, HEK293-mock; red, HEK293-hP2X$_7$R clone A; green, HEK293-hP2X$_7$R clone B; light blue, HEK293-hP2X$_7$R clone C; dark blue, HEK293-rP2X$_7$R; cyan, HEK293-rP2X$_7$ΔC. ***$p \leq 0.0001$ versus HEK293-mock.

without being first translated into a significant increase of the average $[Ca^{2+}]_i$. This might occur via an increased Ca^{2+} influx from the extracellular space through the ER to the mitochondria. This pathway seems to be mainly operative under resting conditions, when the P2X$_7$R undergoes tonic, low level activation. On the contrary, when the receptor is fully activated, the very large Ca^{2+} influx occurring through this high conductance pathway bypasses the ER, and Ca^{2+} is directly taken up by the mitochondria. The fact that expression of P2X$_7$ΔCR, which has a lower Ca^{2+} conductance, has little effect on basal $[Ca^{2+}]_{mt}$, may imply that Ca^{2+} influx across this truncated receptor is too small to cause localized $[Ca^{2+}]_i$ increases or that deletion of the COOH tail prevents a close interaction between P2X$_7$R and the mitochondrial network.

Mitochondrial dysfunction is increasingly recognized as a crucial step in the initiation or progression of apoptosis (Bernardi *et al.*, 2001). Although it is still debated whether a $\Delta\psi_{mt}$ collapse is absolutely needed, it is clear that a $\Delta\psi_{mt}$ drop and an increase in $[Ca^{2+}]_{mt}$ are generally associated to release of cytochrome *c*, AIF, and SMAC/Diablo from the mitochondria (Kroemer and Reed, 2000). This suggests that cells with a higher $\Delta\psi_{mt}$ should be more resistant to apoptosis, i.e., have a growth/survival advantage. A recent study reports that, among human colonic carcinoma cells, those with an intrinsic higher $\Delta\psi_{mt}$ release less cytochrome *c* and are more resistant to apoptosis (Heerdt *et al.*, 2003). Along these same lines, overexpression of the human mitochondrial form of thioredoxin, a protein overexpressed in several brain tumors, induces an increase of $\Delta\psi_{mt}$ and enhances ATP synthesis in HEK293 cells (Damdimopoulos *et al.*, 2002).

We are presented with a completely different scenario when the P2X$_7$R is maximally stimulated by extracellular ATP: now the cell cytoplasm is flooded with Ca^{2+} and massive Ca^{2+} uptake occurs into the mitochondria. The mitochondria cannot cope with Ca^{2+} overload, the $\Delta\psi_{mt}$ collapses, the mitochondrial network is fragmented and the cell, unless extracellular ATP is quickly removed and the P2X$_7$R channel closes, is bound to die. As yet, the determi-

nants of the proliferation/death dicotomic choice are unknown, but mitochondria might be a central player, depending on their ability/inability to cope with the Ca^{2+} overload.

In conclusion, we show here that expression and basal activation of the P2X$_7$R modulates mitochondrial ion homeostasis and increases cellular energy stores. This enhanced metabolic status correlates with a better survival of P2X$_7$R transfectants in the absence of growth factors. Contrarywise, a strong stimulation of the P2X$_7$R causes a dramatic overflow of $[Ca^{2+}]_{mt}$, $\Delta\psi_{mt}$ collapse, extensive fragmentation of the mitochondrial network, and cell death. These observations help understand the mechanism of the dual effect of P2X$_7$R stimulation on cell growth and cell death and provide a mechanism by which basal activation of a plasma membrane pore acting at the mitochondria may enhance cell proliferation.

ACKNOWLEDGMENTS

REFERENCES

Adinolfi, E., Kim, M., Young, M. T., Di Virgilio, F., and Surprenant, A. (2003). Tyrosine phosphorylation of HSP90 within the P2X7 receptor complex negatively regulates P2X7 receptors. J. Biol. Chem. *278*, 37344–37351.

Adinolfi, E., Melchiorri, L., Falzoni, S., Chiozzi, P., Morelli, A., Tieghi, A., Cuneo, A., Castoldi, G., Di Virgilio, F., and Baricordi, O. R. (2002). P2X7 receptor expression in evolutive and indolent forms of chronic B lymphocytic leukemia. Blood *99*, 706–708.

Baricordi, O. R., Melchiorri, L., Adinolfi, E., Falzoni, S., Chiozzi, P., Buell, G., and Di Virgilio, F. (1999). Increased proliferation rate of lymphoid cells transfected with the P2X$_7$ ATP receptor. J. Biol. Chem. *274*, 33206–33208.

Bernardi, P., Petronilli, V., Di Lisa, F., and Forte, M. (2001). A mitochondrial perspective on cell death. Trends Biochem. Sci. *26*, 112–117.

Burnstock, G. (2002). Purinergic signalling and vascular cell proliferation and death. Arterioscler. Thromb. Vasc. Biol. *22*, 364–373.

Damdimopoulos, A. E., Miranda-Vizuete, A., Pelto-Huikko, M., Gustafsson, J. A., and Spyrou, G. (2002). Human mitochondrial thioredoxin. Involvement in mitochondrial membrane potential and cell death. J. Biol. Chem. *277*, 33249–33257.

Denton, R. M., and McCormack, J. M. (1980). On the role of the calcium transport cycle in heart and other mammalian mitochondria. FEBS Lett. *119*, 1–8.

Di Virgilio, F. (1995). The P2Z purinoceptor: an intriguing role in immunity, inflammation and cell death. Immunol. Today *16*, 524–528.

Di Virgilio, F., Chiozzi, P., Ferrari, D., Falzoni, S., Sanz, J. M., Morelli, A., Torboli, M., Bolognesi, G., and Baricordi, O. R. (2001). Nucleotide receptors: an emerging family of regulatory molecules in blood cells. Blood *97*, 587–600.

Duchen, M. R., Surin, A., and Jacobson, J. (2003). Imaging mitochondrial function in intact cells. Methods Enzymol. *361*, 353–389.

Fabbro, A., Skorinkin, A., Grandolfo, M., Nistri, A., and Giniatullin, R. (2004). Quantal release of ATP from clusters of PC12 cells. J. Physiol. *560*, 505–517.

Falzoni, S., Munerati, M., Ferrari, D., Spisani, S., and Di Virgilio, F. (1995). The purinergic P2Z receptor of human macrophages: characterization and possible physiological role. J. Clin. Investig. *95*, 1207–1216.

Ferrari, D., Pizzirani, C., Adinolfi, E., Forchap, S., Sitta, B., Turchet, L., Falzoni, S., Minelli, M., Baricordi, O. R., and Di Virgilio, F. (2004). The antibiotic polymyxin B modulates P2X7 receptor function. J. Immunol. *173*, 4652–4660.

Greig, A. V., Linge, C., Healy, V., Lim, P., Clayton, E., Rustin, M. H., McGrouther, D. A., and Burnstock, G. (2003). Expression of purinergic receptors in non-melanoma skin cancers and their functional roles in A431 cells. J. Investig. Dermatol. *121*, 315–327.

Heerdt, B. G., Houston, M. A., Wilson, A. J., and Augenlicht, L. H. (2003). The intrinsic mitochondrial membrane potential (Deltapsim) is associated with steady-state mitochondrial activity and the extent to which colonic epithelial cells undergo butyrate-mediated growth arrest and apoptosis. Cancer Res. *63*, 6311–6319.

Joseph, S. M., Buchakjian, M. R., and Dubyak, G. R. (2003). Colocalization of ATP release sites and ecto-ATPase activity at the extracellular surface of human astrocytes. J. Biol. Chem. *278*, 23331–23342.

Jouaville, L. S., Pinton, P., Bastianutto, C., Rutter, G. A., and Rizzuto, R. (1999). Regulation of mitochondrial ATP synthesis by calcium: evidence for a long-term metabolic priming. Proc. Natl. Acad. Sci. USA *96*, 13807–13812.

Kim, M., Jiang, L. H., Wilson, H. L., North, R. A., and Surprenant, A. (2001). Proteomic and functional evidence for a P2X7 receptor signalling complex. EMBO J. *20*, 6347–6358.

Kroemer, G., and Reed, J. C. (2000). Mitochondrial control of cell death. Nat. Med. *6*, 513–519.

MacKenzie, A., Wilson, H. L., Kiss-Toth, E., Dower, S. K., North, R. A., and Surprenant, A. (2001). Rapid secretion of interleukin-1beta by microvesicle shedding. Immunity *15*, 825–835.

Morelli, A., Chiozzi, P., Chiesa, A., Ferrari, D., Sanz, J. M., Falzoni, S., Pinton, P., Rizzuto, R., Olson, M. F., and Di Virgilio, F. (2003). Extracellular ATP causes ROCK I-dependent bleb formation in P2X7-transfected HEK293 cells. Mol. Biol. Cell *14*, 2655–2664.

North, R. A. (2002). Molecular physiology of P2X receptors. Physiol. Rev. *82*, 1013–1067.

Rassendren, F., Buell, G. N., Virginio, C., Collo, G., North, R. A., and Surprenant, A. (1997). The permeabilizing ATP receptor, P2X7. Cloning and expression of a human cDNA. J. Biol. Chem. *272*, 5482–5486.

Rizzuto, R., Bastianutto, C., Brini, M., Murgia, M., and Pozzan, T. (1994). Mitochondrial Ca^{2+} homeostasis in intact cells. J. Cell Biol. *126*, 1183–1194.

Rizzuto, R., Bernardi, P., and Pozzan, T. (2000). Mitochondria as all-round players of the calcium game. J. Physiol. *529*, 37–47.

Rizzuto, R., Brini, M., Murgia, M., and Pozzan, T. (1993). Microdomains with high Ca^{2+} close to IP_3-sensitive channels that are sensed by neighboring mitochondria. Science *262*, 744–747.

Rizzuto, R., Brini, M., Pizzo, P., Murgia, M., and Pozzan, T. (1995). Chimeric green fluorescent protein as a tool for visualizing subcellular organelles in living cells. Curr. Biol. *5*, 635–642.

Rizzuto, R., Carrington, W., and Tuft, R. A. (1998). Digital imaging microscopy of living cells. Trends Cell Biol. *8*, 288–292.

Scaduto, R. C., Jr., and Grotyohann, L. W. (1999). Measurement of mitochondrial membrane potential using fluorescent rhodamine derivatives. Biophys. J. *76*, 469–477.

Slater, M., Danieletto, S., Gidley-Baird, A., Teh, L. C., and Barden, J. A. (2004). Early prostate cancer detected using expression of non-functional cytolytic P2X7 receptors. Histopathology *44*, 206–215.

Surprenant, A., Rassendren, F., Kawashima, E., North, R. A., and Buell, G. (1996). The cytolytic P2Z receptor for extracellular ATP identified as a P2X receptor ($P2X_7$). Science *272*, 735–738.